BJR, 2024, **97**, 734–743
https://doi.org/10.1093/bjr/tqae016
Advance access publication: 16 January 2024
Pictorial Review

Imaging characterization of paediatric tumours with the *neurotrophic tyrosine receptor kinase* fusion transcript

Anne-Laure Hermann , MD[1,*], Lauriane Lemelle, MD[2], Gaëlle Pierron , PhD[3], Arnaud Gauthier, MD[4], Nayla Nicolas, MD[1], Liesbeth Cardoen, MD, PhD[1], Salma Moalla, MD[5], Philippe Petit, MD, PhD[6], Baptiste Morel, MD, PhD[7], Hubert Ducou Le Pointe, MD, PhD[8], Adnan Hassani, MD[9], Paul Fréneaux, MD[4], Delphine Guillemot, MD[3], Matthieu Carton, MD, PhD[10], Nadège Corradini, MD, PhD[11], Angélique Rome, MD[12], Marie-Pierre Castex, MD[13], Anne-Sophie Defachelles, MD[14], Gudrun Schleiermacher, MD, PhD[2], Pablo Berlanga, MD[15], Olivier Delattre, MD, PhD[2,3], Daniel Orbach , MD, PhD[2], Hervé J. Brisse, MD, PhD[1]

[1]Department of Imaging, Institut Curie, PSL University, Paris, 75005, France
[2]SIREDO Oncology Center (Care, Innovation and Research for Children and AYA with Cancer), Institut Curie, PSL University, Paris, 75005, France
[3]Department of Somatic Genetics, Institut Curie, PSL University, Paris, 75005, France
[4]Department of Pathology, Institut Curie, PSL University, Paris, 75005, France
[5]Department of Imaging, Gustave Roussy Cancer Center, Villejuif, 94805, France
[6]Department of Imaging, Assistance Publique des Hôpitaux de Marseille, Hôpital de La Timone, Marseille, 13005, France
[7]Department of Pediatric Radiology, CHRU Hôpitaux de Tours, Tours, 37000, France
[8]Department of Pediatric Radiology, Assistance Publique des Hôpitaux de Paris, Hôpital Armand Trousseau, Paris, 75012, France
[9]Department of Pediatric Radiology, CHU Rouen, Rouen, 76000, France
[10]Department of Biostatistics, Institut Curie, PSL University, Paris, 75005, France
[11]Department of Pediatric Oncology and Hematology, Centre Léon Bérard, Lyon, 69008, France
[12]Department of Pediatric Oncology, Assistance Publique des Hôpitaux de Marseille, Hôpital de la Timone, Marseille, 13005, France
[13]Department of Pediatric Oncology and Hematology, CHU Toulouse, Toulouse, 31300, France
[14]Department of Pediatric Oncology, Oscar Lambret Center, Lille, 59000, France
[15]Department of Pediatric and Adolescent Oncology, Gustave Roussy Cancer Center, INSERM U1015, Université Paris-Saclay, Villejuif, 94805, France

*Corresponding author: Anne-Laure Hermann, MD, Department of Imaging, Institut Curie, Paris, France, 25 rue d'Ulm, Paris 75005 (Annelaure.hermann@gmail.com; anne-laure.hermann@chu-lyon.fr)

Abstract

Objectives: The *neurotrophic tyrosine receptor kinase (NTRK)* fusion transcript (FT) is a major genetic landmark of infantile fibrosarcoma (IFS) and cellular congenital mesoblastic nephroma (cCMN) but is also described in other tumours. The recent availability of *NTRK*-targeted drugs enhances the need for better identification. We aimed to describe the anatomic locations and imaging features of tumours with *NTRK*-FT in children.

Case series: Imaging characteristics of *NTRK*-FT tumours of 41 children (median age: 4 months; 63% <1 year old; range: 0-188) managed between 2001 and 2019 were retrospectively analysed. The tumours were located in the soft tissues ($n=24$, including 19 IFS), kidneys ($n=9$, including 8 cCMN), central nervous system (CNS) ($n=5$), lung ($n=2$), and bone ($n=1$). The tumours were frequently deep-located (93%) and heterogeneous (71%) with necrotic (53%) or haemorrhagic components (29%). Although inconstant, enlarged intratumoural vessels were a recurrent finding (70%) with an irregular distribution (63%) in the most frequent anatomical locations.

Conclusion: Paediatric *NTRK*-FT tumours mainly occur in infants with very variable histotypes and locations. Rich and irregular intra-tumoural vascularization are recurrent findings.

Advances in knowledge: Apart from IFS of soft tissues and cCMN of the kidneys, others *NTRK*-FT tumours locations have to be known, as CNS tumours. Better knowledge of the imaging characteristics may help guide the pathological and biological identification.

Keywords: neurotrophic tyrosine receptor kinase; fusion transcript tumour; infantile fibrosarcoma; cellular congenital mesoblastic nephroma; MRI.

Introduction

The family of transmembrane tyrosine receptor kinases (TRKA, TRKB, TRKC) is encoded by the *NTRK1*, *NTRK2*, *and NTRK3* genes, which are critical players in neural development. Gene fusions involving *NTRK* lead to a fusion protein comprising the kinase domain of the TRK protein, which is a driver of pro-oncogenic pathways. These genetic alterations have been described in approximately 0.3% of all solid tumours, 0.3% of adult tumours, and 1.3% of paediatric tumours.,[1] In paediatric tumours, *NTRK*-fusion transcripts (*NTRK*-FT) were first described with the *ETV6* partner gene (*ETV6::NTRK3*) in congenital/infantile fibrosarcoma (IFS)[2] and cellular congenital mesoblastic nephromas (cCMN).[3] Other *NTRK* partners (*EML4::NTRK3*, *TMP3::NTRK1*, *LMNA::NTRK1*, and *SCYL3::NTRK1*) were further identified in various malignant tumours. The recent development of efficient drugs (eg, Larotrectinib) blocking the *NTRK* molecular pathway provided critical hope for treating these tumours.[4,5] However, little is known about their imaging features apart from IFS,[6,7] a small series of cCMN,[8] and case

Received: 28 June 2023; **Revised:** 12 December 2023; **Accepted:** 12 January 2024

reports of non-IFS soft tissue *NTRK*-rearranged neoplasms.[9-11] Until now, the radiological features of all *NTRK*-FT tumours, regardless of their anatomical location, have not been described and compared. The present study was aimed to collect a series of paediatric tumours with *NTRK*-FT and describe both their anatomic locations and imaging features for better identification.

Case series

Patient cohort

Forty-one patients managed between 2001 and 2019 in 13 different centres were included for this retrospective analysis. Twenty-two (54%) were male, and 19 (46%) were female. The median patient age at diagnosis was 4 months [range: 0-188 m], and 63% were aged younger than 1 year. All tumours exhibited *NTRK*-FT as assessed by RT-qPCR or RNA sequencing.

This study obtained institutional review board approval. Nonoppositional patient agreement to the study was obtained from their legal guardians.

Tumour locations, histologic subtypes, and genetics

The molecular characteristics of the 41 tumours with *NTRK*-FT are presented in Table 1.

Imaging characteristics

Ultrasound (US), CT-scan, and MRI images were available for retrospective radiological review (by two radiologists by consensus) for 14 (35%), 28 (68%), and 29 patients (71%), respectively. Imaging characteristics of all *NTRK* tumours and of the most frequent location and histotypes are described in Table 2.

Among soft tissue IFSs, approximately half of the cases (53%) had ill-defined margins. Most (79%) were heterogeneous with necrosis (63%) or haemorrhage (47%). Enlarged intratumoural vessels were observed in 89% of cases, with an irregular distribution in 78% and significant enhancement on MRI in 80%. A histological comparison was obtained in one case and confirmed the presence of highly condensed anarchic vascularization composed of irregular thin-walled vessels (Figure 1). Perilesional invasion was found in 68% of the cases with predominantly fat invasion (69%) (Figures 1-3).

The cCMNs were large tumours at diagnosis with a median tumour volume of 263 cm^3 (IQR: 47-569) and a median largest diameter of 85 mm (IQR: 50-150). Only US (50%) or CT (100%) were available for these tumours. They were heterogeneous (88%) with necrosis (63%) or haemorrhage (25%), and no calcification or fibrosis was identified. Additionally, 88% of the cases demonstrated enlarged intratumoural vessels with an irregular distribution in 63% of them. In all the patients, the tumour was confined to the kidney without surrounding tissue invasion and without metastatic lesions (Figures 4 and 5).

The CNS tumours included four brain tumours and one spinal tumour. Among the brain tumours, three were large masses at diagnosis with a median largest diameter of 72 mm (IQR: 58-78); the other tumour was a centimetric pineal embryonal malignant tumour. Two of the tumours were heterogeneous (with necrosis and haemorrhagic components) and displayed marked enhancement of the tissue portion (Figures 6 and 7). The other tumour demonstrated no tissue enhancement but enlarged intratumoural and peritumoural vessels (Figure 8). All the tumours had well-defined margins. They showed a mass effect on the surrounding parenchyma and ventricles, except for the mass located in the pineal gland due to its smaller size. Only one tumour demonstrated white matter perilesional oedema (Figure 6). The spinal tumour was a diffuse leptomeningeal glioneuronal tumour harbouring an *NTRK2-AGAP1* fusion transcript in a 12-year-old boy. On imaging, it appeared as an infiltrative lesion of the spinal cord containing cystic components and highly enhanced tissue portions (Figure 9).

The five other tumours located in the soft tissues showed various imaging aspects, most of them demonstrating high enhancement (80%) with focal invasiveness into the surrounding tissues, especially fat tissue (80%). One benign dendrocyte hamartoma was located in the subcutaneous fat of the scalp, and the other was located in the subcutaneous fat and muscular part of the abdominal wall (Figure 10). The two benign mesenchymal tumours (both harbouring both *TPM3::NTRK1* fusion transcripts) presented as a homogeneous and highly vascularized anoperineal mass and as a

Table 1. Tumour molecular characteristics of the 41 tumours with NTRK-FT.

Anatomical location	Histology	Fusion partners	Number (%)
Soft tissue (*n* = 24)	Infantile fibrosarcoma	*NTRK3-ETV6*	18 (44)
		NTRK1-TPR	1 (2.5)
	Benign dendrocyte hamartoma	*NTRK3-KHDRBS1*	1 (2.5)
		NTRK3-EML4	1 (2.5)
	Benign mesenchymal tumour	*NTRK1-TPM3*	2 (5)
	Lipofibromatosis-like neural tumour	*NTRK1-TPM3*	1 (2.5)
Kidney (*n* = 9)	Cellular congenital mesoblastic nephroma	*NTRK3-ETV6*	8 (19)
	Renal undifferentiated sarcoma	*NTRK1-LMNA*	1 (2.5)
Central nervous system (*n* = 5)	Embryonal malignant tumour	*NTRK1-TPM3*	1 (2.5)
		NTRK2-KANK2	1 (2.5)
	High-grade glioma	*NTRK2-BCR*	1 (2.5)
	Atypical teratoid rhabdoid tumour	*NTRK3-SPECC1*	1 (2.5)
	Spinal leptomeningeal glioneuronal tumour	*NTRK2-AGAP1*	1 (2.5)
Lung (*n* = 2)	Inflammatory myofibroblastic tumour	*NTRK3-ETV6*	1 (2.5)
	Lung undifferentiated sarcoma	*NTRK3-ETV6*	1 (2.5)
Bone (*n* = 1)	Osteosarcoma	*NTRK3-CAMSAP2*	1 (2)
Total			**41 (100)**

Table 2. Imaging characteristics of all NTRK tumours, soft-tissue IFS, renal cCMN, soft-tissue non-IFS and brain tumours with NTRK-FT.

	Criteria	All NTRK-FT tumours ($n = 41$)	Soft-tissue IFS ($n = 19$)	Renal cCMN ($n = 8$)	Soft-tissue non-IFS ($n = 5$)	Brain tumours ($n = 4$)
Age at diagnosis	Median, range (months)	4 m [0-188]	2 m [0-74]	3.5 m [1-20]	2 (40%)	76 m [2-156]
Gender	Boys/girls	22/19	10/9	6/2	3 (60%)	3/1
Location	Superficial	3 (7%)	1 (5%)	0 (0%)	43 (IQR 20-82)	0 (0%)
	Deep	38 (93%)	18 (95%)	8 (100%)	14.5 (4-91)	4 (100%)
Tumour size	Median of largest diameter (mm)	65 (IQR 11-154)	50 (IQR 12-118)	85 (IQR 50-150)	2 (40%)	65 (IQR 11-78)
	Median of volume (cm^3)	58 (IQR (0.6-847)	37 (IQR 1-530)	263 (IQR 47-748)	3 (60%)	123 (IQR 1-228)
Margins	Well-defined	21/41 (51%)	10/19 (53%)	3/8 (38%)	5 (100%)	4/4 (100%)
	Ill-defined	20/41 (49%)	9/19 (47%)	5/8 (63%)	0 (0%)	0/4 (0%)
Tumour content	Homogeneous	12/41 (29%)	4/19(21%)	1/8 (13%)	0 (0%)	1/4 (25%)
	Heterogeneous	29/41 (71%)	15/19 (79%)	7/8 (88%)	0 (0%)	3/4 (75%)
	Necrosis	21/40 (53%)	12/19 (63%)	5/8 (63%)	0 (0%)	2/4 (50%)
	Haemorrhage	12/41 (29%)	9/19 (47%)	2/8 (25%)	0 (0%)	1/4 (25%)
	Calcification	4/34 (12%)	2/15 (13%)	0/8 (8%)	1 (20%)	0/3 (0%)
	Fibrosis	1/22 (5%)	0/11 (0%)	0/4 (0%)	0 (0%)	0/2 (0%)
Vascularization pattern	Enlarged peritumoural (afferent/efferent) vessels	22/41 (54%)	13/19 (68%)	3/8 (38%)	1 (20%)	3/4 (75%)
	Enlarged intratumoural vessels	28/40 (70%)	16/18 (89%)	7/8 (88%)	0 (0%)	3/4 (75%)
	Irregular distribution	25/40 (63%)	14/18 (78%)	5/8 (63%)	1 (20%)	3/4 (75%)
MRI enhancement	No enhancement	1/26 (4%)	0/15 (0%)	NA	4 (80%)	1/4 (25%)
	Mild enhancement	7/26 (27%)	3/15 (20%)	NA	4 (80%)	2/4 (50%)
	High enhancement	18/26 (69%)	12/15 (80%)	NA	1 (20%)	1/4 (25%)
	Homogenous	7/25 (28%)	3/15 (20%)	NA	0 (0%)	0/3 (0%)
	Heterogenous	18/25 (72%)	12/15 (80%)	NA	5 (100%)	3/3 (100%)
	Peripheral	2/25 (8%)	1/15 (7%)	NA	0 (0%)	1/3 (33%)
	Central and peripheral	23/25 (92%)	14/15 (93%)	NA	5 (100%)	2/3 (67%)
Perilesional invasion	No	18/41 (44%)	6/19 (32%)	8/8 (100%)	4 (80%)	1/4 (25%)
	Yes	23/41 (56%)	13/19 (68%)	0/8 (0%)	2 (40%)	3/4 (75%)
	Fat invasion	13/23 (57%)	9/13 (69%)	NA	1 (20%)	0/4 (0%)
	Bone invasion	8/23 (35%)	5/13 (38%)	NA	1 (20%)	0/4 (0%)
	Vascular/muscular/nervous invasion	9/23 (39%)	7/13 (54%)	NA	0 (0%)	0/4 (0%)
	Others	4/23 (17%)	0/13 (0%)	NA	0 (0%)	3/3 (100%)

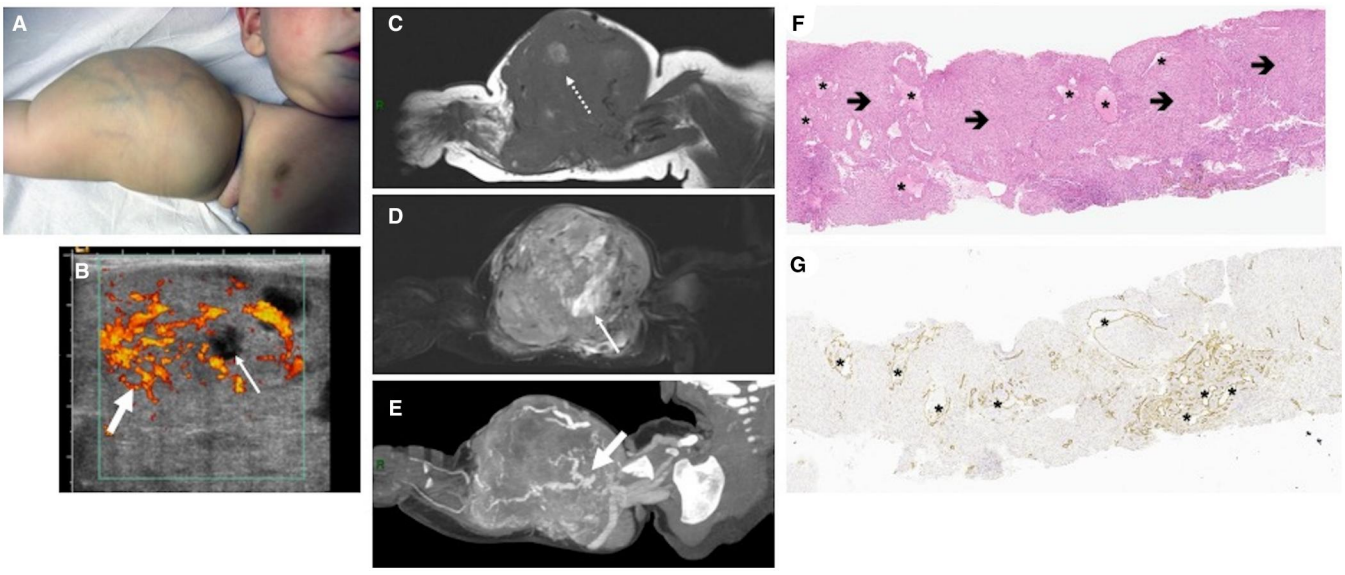

Figure 1. IFS with the ETV6-NTRK3 fusion transcript in the right arm of a 4-month-old boy. (A) Clinical examination demonstrated a large mass in the right arm, with subcutaneous vascularization. (B) Longitudinal power Doppler US demonstrated a heterogeneous mass with irregular vascularization (thick arrow) and necrosis, apparent as a nonvascularized hypoechoic area (arrow). (C) Coronal T1-weighted MR imaging demonstrated an area of hyperintense haemorrhage within the lesion (dotted arrow). (D) The coronal T2-weighted MR image shows a heterogeneous mass with partial necrosis (arrow). (E) The coronal reconstruction with maximum intensity projection (MIP) postprocessing of the CT image shows enlarged peritumoural and intratumoural vessels (thick arrow). Histological views from the core needle biopsy specimen (F) H&E, 10×. Highly condensed anarchic vascularization composed of irregular thin-walled vessels (*) within proliferating spindle cells (→). (G) CD31, 10×. Highlighted vascularization (*) through endothelial cell staining (brown).

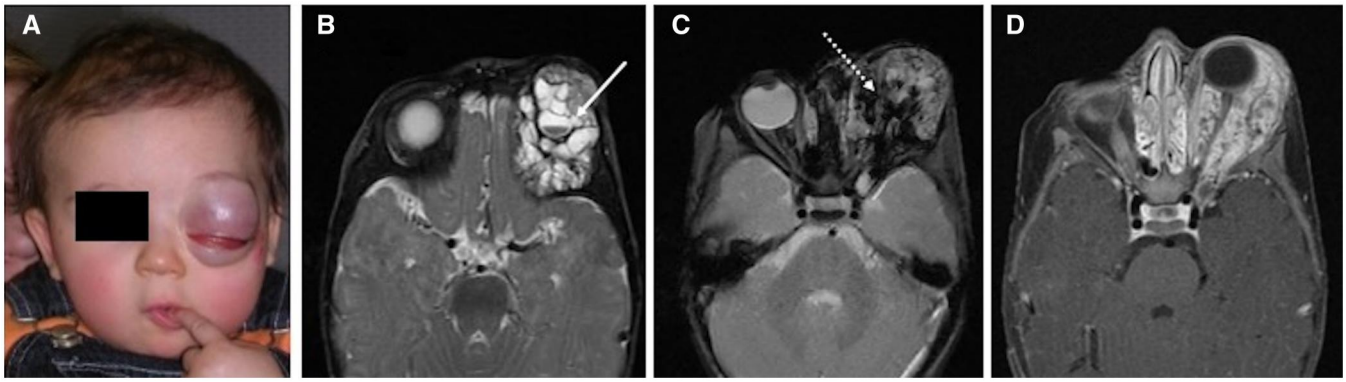

Figure 2. Orbital IFS with the *ETV6-NTRK3* fusion transcript in a 2-month-old boy. (A) Clinical examination demonstrated a large orbital mass with exophthalmia. (B) The axial T2-weighted MR image shows a large heterogeneous orbital mass containing fluid areas with liquid/liquid levels (arrow). (C) The axial T2*-weighted MR image demonstrates haemorrhagic components (dotted arrow). (D) The axial postcontrast T1-weighted fat-saturated MR image shows marked and heterogeneous enhancement and enlarged high-flow vessels.

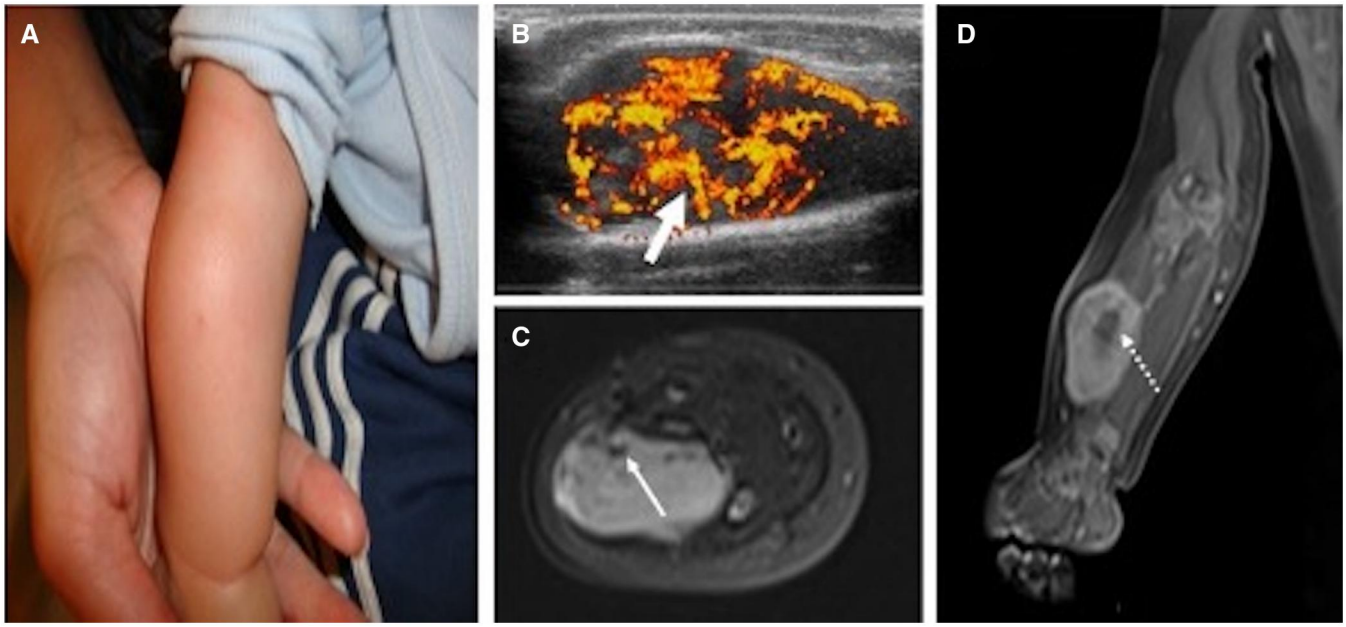

Figure 3. Forearm IFS with ETV6-NTRK3 fusion transcript in a 5-month-old boy. (A) Clinical examination demonstrated a soft-tissue mass without skin alteration. (B) Longitudinal power Doppler US showed a subaponeurotic mass with high vascularization exhibiting an irregular distribution (thick arrow). (C) The axial T2-weighted fat-saturated MR image shows flow voids within the lesion (arrow). (D) The coronal postcontrast T1-weighted fat-saturated MR image shows heterogeneous enhancement of the lesion with central nonenhanced necrosis (dotted arrow).

subaponeurotic homogeneous and poorly vascularized mass of the leg. The low-grade spindle cell sarcoma/lipofibromatosis-like neural tumour was located in the paravertebral muscles with an epidural extension and appeared as a homogeneous infiltrative mass with marked enhancement and invasion of the surrounding bone (Figure 11).

The other tumour located in the kidney was an undifferentiated sarcoma with an *LMNA::NTRK3* fusion transcript in a 12-year-old boy presenting as a large highly vascularized mass with extensive necrosis and pulmonary and spinal leptomeningeal metastases (Figure 12).

The two lung tumours had both *ETV6::NTRK3* fusion transcripts. Undifferentiated sarcoma in a 10-year-old boy presented as a well-defined mass containing central necrosis and enlarged intratumoural and afferent vessels. The other tumour was an *ALK*-negative inflammatory myofibroblastic tumour in a 15-month-old girl and presented as a well-defined solid mass with pronounced peripheral enhancement but without abnormally enlarged vessels (Figure 13).

The only bone tumour case was an osteosarcoma of the fibula in a 15-year-old girl that harboured the *CAMSAP2::NTRK3* fusion transcript with no difference on imaging compared with conventional osteosarcoma (Figure 14).

Discussion

According to our cohort, paediatric *NTRK*-FT tumours mainly occur in infants, with the most frequent anatomical locations being soft tissues (59%) and kidneys (22%), while the CNS (12%) appeared as the next most frequent site of origin. The most common imaging findings were deep location (93%), heterogeneity (71%), enlarged (70%), and irregular

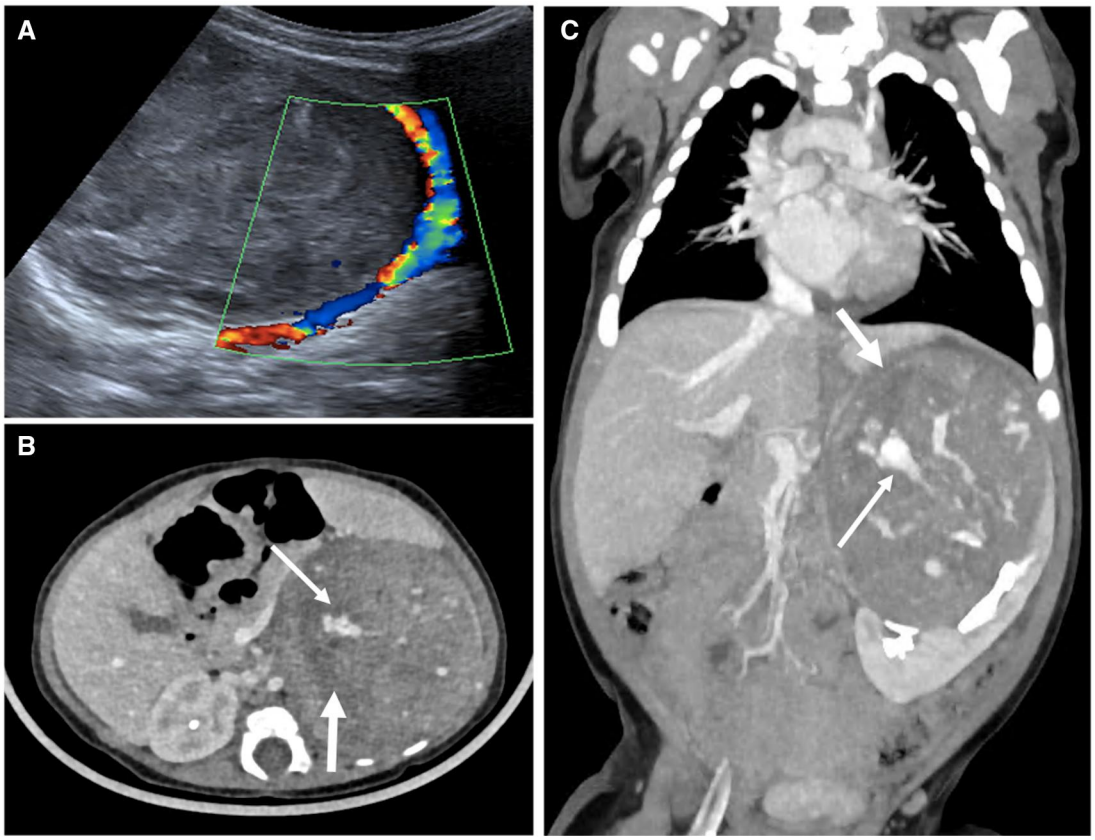

Figure 4. Cellular congenital mesoblastic nephroma with the *ETV6-NTRK3* fusion transcript in a 5-month-old boy. Transverse colour-Doppler mode US (A) and contrast-enhanced CT at the portal phase on the axial (B) and coronal views (C). A large heterogeneous mass containing a hypointense area (thick arrow) and highly vascularized tissue portions was observed displaying very enlarged intratumoural vessels with an irregular distribution (arrow) and enlarged peripheral vessels (A). No invasion of the surrounding tissues was observed.

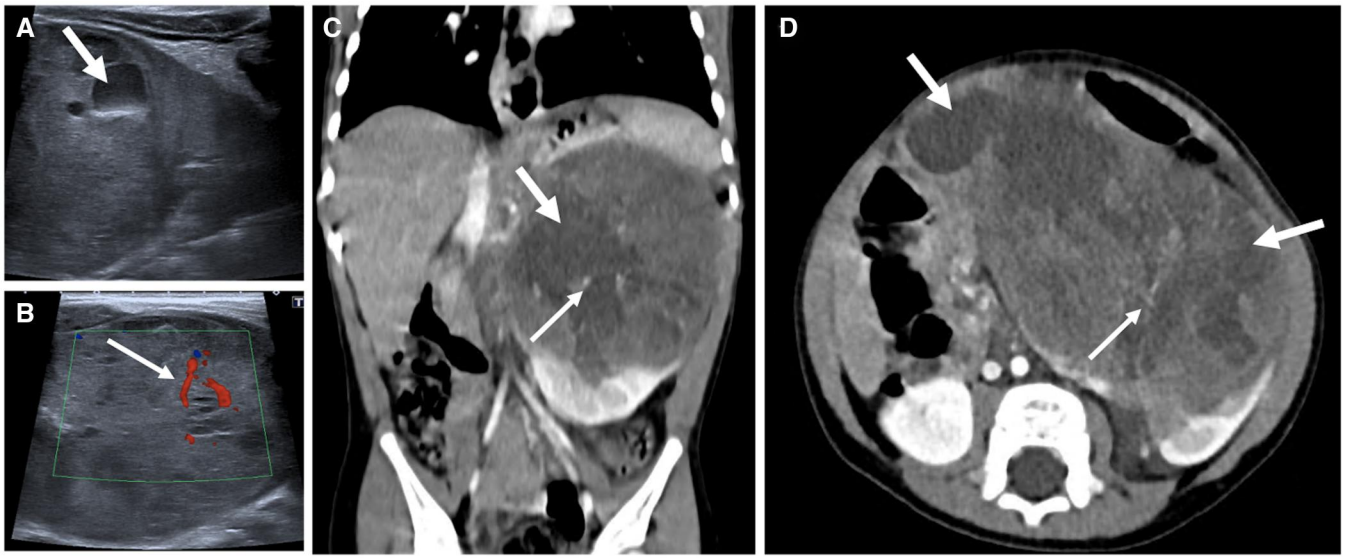

Figure 5. Cellular congenital mesoblastic nephroma with *ETV6-NTRK3* fusion transcript in a 20-month-old boy. Transverse greyscale (A) and longitudinal Doppler colour mode (B) US and contrast-enhanced CT in the portal phase in the coronal view (C) and axial view (D). A large and heterogeneous mass of the left kidney is demonstrated; the mass contained a large portion of nonenhanced liquid necrosis (thick arrow) and displayed enlarged intratumoural vessels (thin arrow).

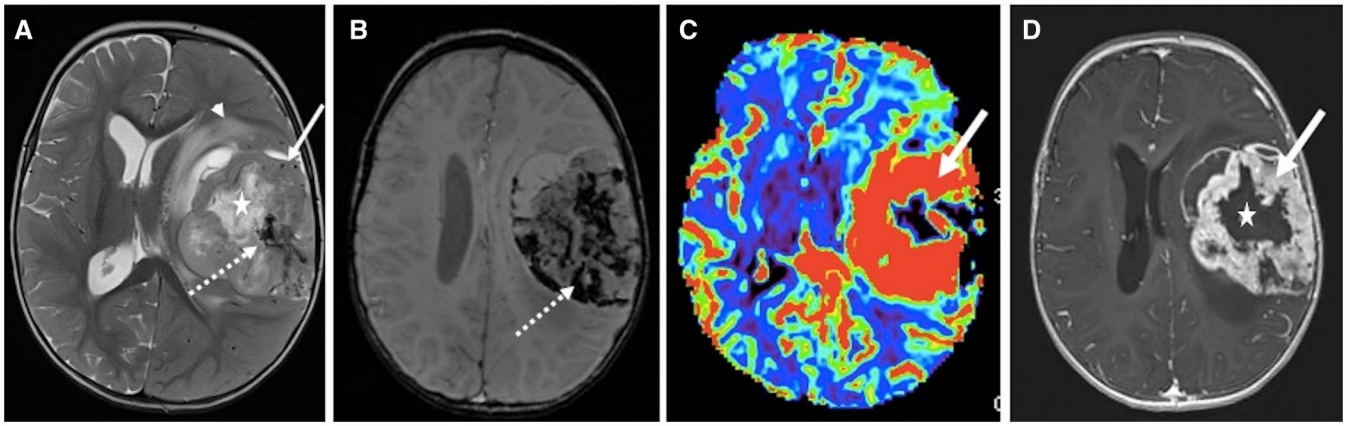

Figure 6. Atypical teratoid rhabdoid tumour (ATRT) with the *NTRK3-SPECC1* fusion transcript in a 15-month-old boy. Axial T2 (A), SWI (B), ASL (C), and postcontrast T1 (D) weighted MRI images reveal a large frontoparietal intra-axial well-defined mass with a central portion of necrosis (star) and haemorrhage (dotted arrow), containing flow voids on T2 (thin arrow) and displaying high, heterogeneous and peripheral enhancement with increased perfusion on ASL (thick arrow). Perilesional oedema of the surrounding white matter (arrowhead) was observed.

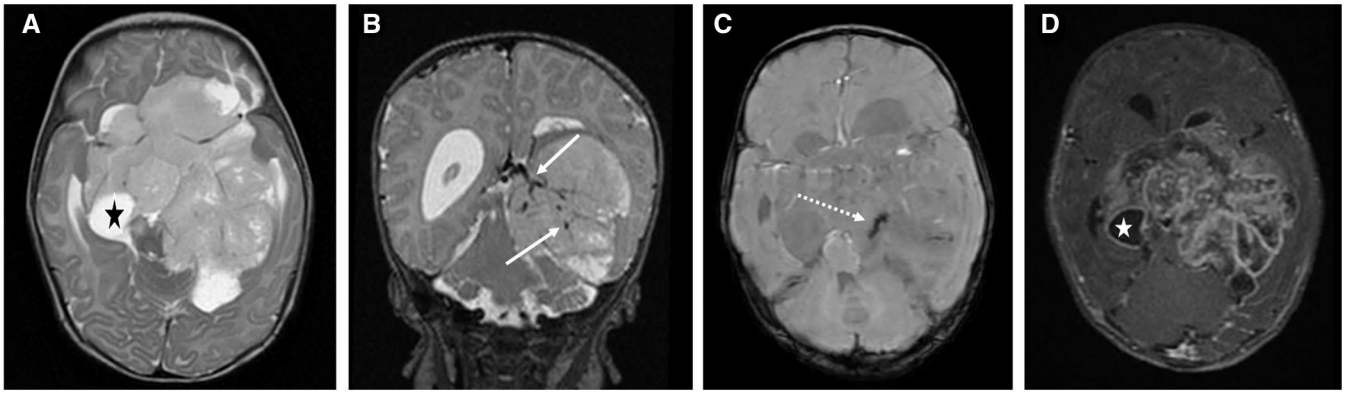

Figure 7. High-grade glioma with the NTRK2-BCR fusion transcript in a 2-month-old girl. Axial T2 (A), coronal T2 (B), axial SWAN (C), and postcontrast T1 (D)-weighted MR images. MR revealed a large infiltrative intra-axial mass with frontotemporal invasion, containing fluid portions (star), a small haemorrhagic component (dotted arrow), enlarged afferent and intratumoural vessels (arrow) with mild, heterogeneous central and peripheral enhancement.

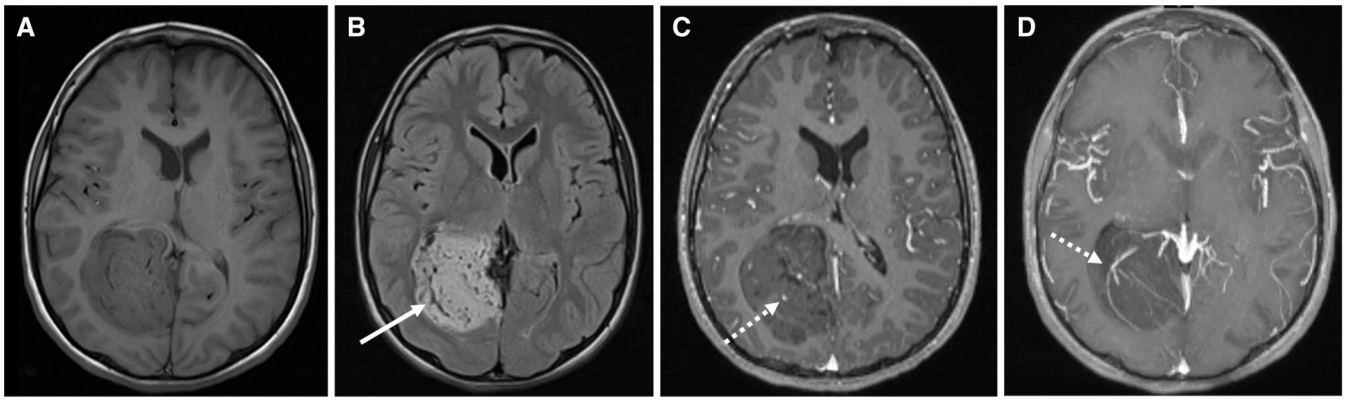

Figure 8. Embryonal malignant CNS tumour with the NTRK1-TMP3 fusion transcript in a 12-year-old boy. Axial T1 (A), axial FLAIR (B), axial postcontrast T1 (C), and axial postcontrast T1 with maximum intensity projection (MIP) (D) weighted MR images. MR revealed an intra-axial occipital well-defined mass, with no enhancement but containing multiple hypointense flow voids on FLAIR images (arrow), enlarged vessels within and at the periphery of the lesion (dotted arrow).

(63%) intratumoural vascularization and marked enhancement (69%).

IFS has been previously described as exhibiting heterogeneous signal and enhancement related to haemorrhage and necrosis, rare calcifications and extensions into adjacent structures,[12,13] which is consistent with our findings. The vascularization pattern of IFS has not been precisely described in the MR literature thus far. Our series demonstrated

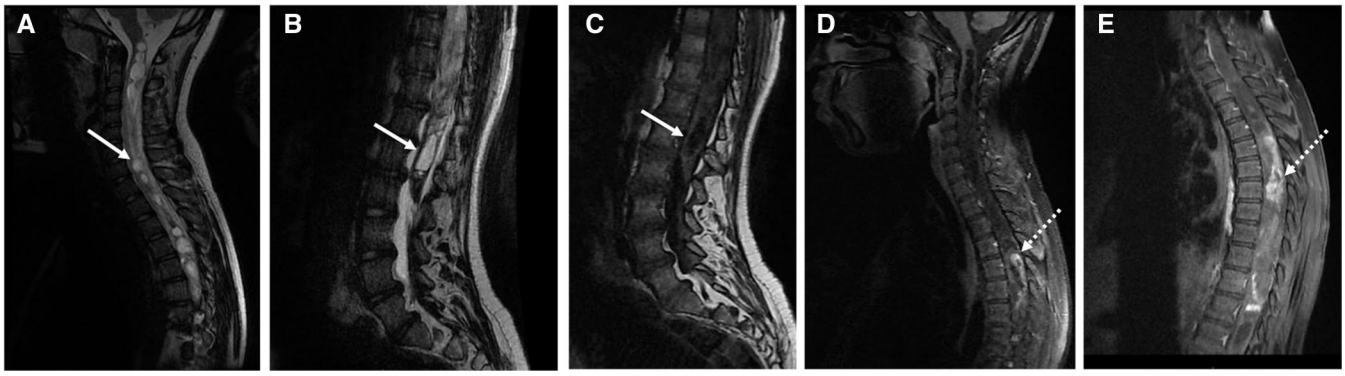

Figure 9. Spinal diffuse leptomeningeal glioneuronal tumour with the NTRK2-AGAP1 fusion transcript in a 12-year-old boy. Medullar sagittal T2 (A, B) sagittal T1 (C) and postcontrast fat-saturated T1 (D, E) weighted MR images show an infiltrative mass along the spinal cord, with ill-defined margins, containing cystic components (arrow) and tissue portions with high and heterogeneous enhancement (dotted arrow).

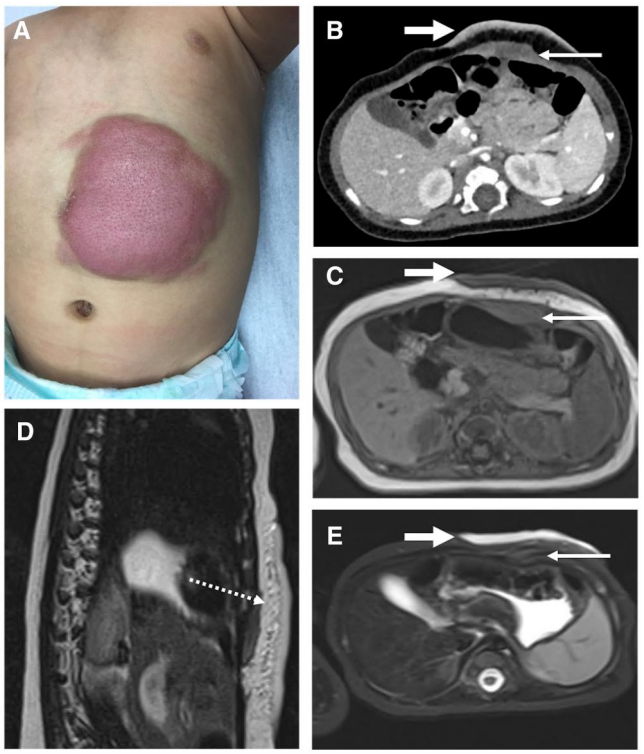

Figure 10. Benign dendrocytic hamartoma of the abdominal wall with the NTRK3-KHDRBS1 fusion transcript in a 4-month-old girl. (A) Clinical examination revealed a large superficial purplish lesion of the skin of the abdominal wall with skin thickening and ill-defined margins. Axial contrast-enhanced CT (B), axial T1-weighted (C), and T2-weighted fat-saturated (R) MR images show two portions within the mass. One is located superficially in the skin and subcutaneous fat of the abdominal wall, demonstrating high and homogeneous enhancement, isointensity on the T1-W image and hyperintensity on the T2-W image (thick arrow). The second one is located deeply in the left right rectus muscle, demonstrating no enhancement or isointensity on T1- and T2-W images (arrow). (D) The sagittal T2-weighted image shows infiltration of the subcutaneous fat between the two parts of the lesion (dotted arrow).

an inconsistent but recurrent pattern of abnormal vascularization involving enlarged peri- or intratumoural vessels with an irregular distribution. The marked degree of vascularity in IFS, which has also been described by pathologists, led to a haemangiopericytoma-like vascular pattern, which might explain these radiological features.[14] Such marked vascularization is not specific to IFS and is observed in other paediatric soft tissue sarcomas, such as rhabdomyosarcoma and alveolar soft-part sarcoma. Interestingly, Kobayashi et al also reported a small series of *NTRK*-rearranged spindle cell neoplasms with a similar pattern of high vascularization with intra- and peritumoural flow voids.[9]

The cellular variant of CMN harbouring the *ETV6::NTRK3* gene fusion is an aggressive infantile renal neoplasm associated with possible local recurrence and metastasis. Its imaging appearance in our series is consistent with the literature,[8] showing large and heterogeneous masses without calcification containing areas of necrosis and fluid-filled cysts. Interestingly, we also observed a peculiar vascularization pattern with enlarged and tortuous intratumoural vessels in all but one case (small-sized and homogeneous tumour). This vascular pattern was not previously reported in the radiologic literature except for one case in Bayindir series.[8] A strong haemangiopericytous vascular pattern has also been described in cCMN,[15] possibly explaining this feature.

In our study, central nervous system (CNS) *NTRK*-FT tumours harboured various *NTRK* fusions, but all three cases of *NTRK2* tumours were located in the CNS. CNS tumours with *NTRK* rearrangements have been described in various histological subtypes, such as low- to high-grade gliomas or ganglioglioma.[16] To date, no specific imaging features have been reported. A few cases[17] have shown tumours with well-defined margins, heterogeneous signals with little to no perilesional oedema and enlarged intratumoural vessels, in agreement with our cases. This imaging pattern is uncommon in paediatric CNS tumours but not specific and has also been reported in children with embryonal tumours presenting multi-layered rosettes[18] and high-grade neuroepithelial tumours with *BCL6* corepressor gene internal tandem duplication.[19]

Among non-IFS soft tissue tumours with *NTRK*-FT, one lipofibromatosis-like neural tumour harbouring the *TPM3::NTRK1* fusion partner was observed in an epidural lumbar location, which was comparable to a previous description.[11] The *LMNA::NTRK1* fusion transcript has been reported in low-grade spindle cell sarcoma in peripheral soft tissues in children and young adults,[9] whereas this specific transcript was observed in our cohort in only one case of renal undifferentiated sarcoma.

Our study presents some limitations: It was retrospective, leading to a marked proportion of missing data (30%).

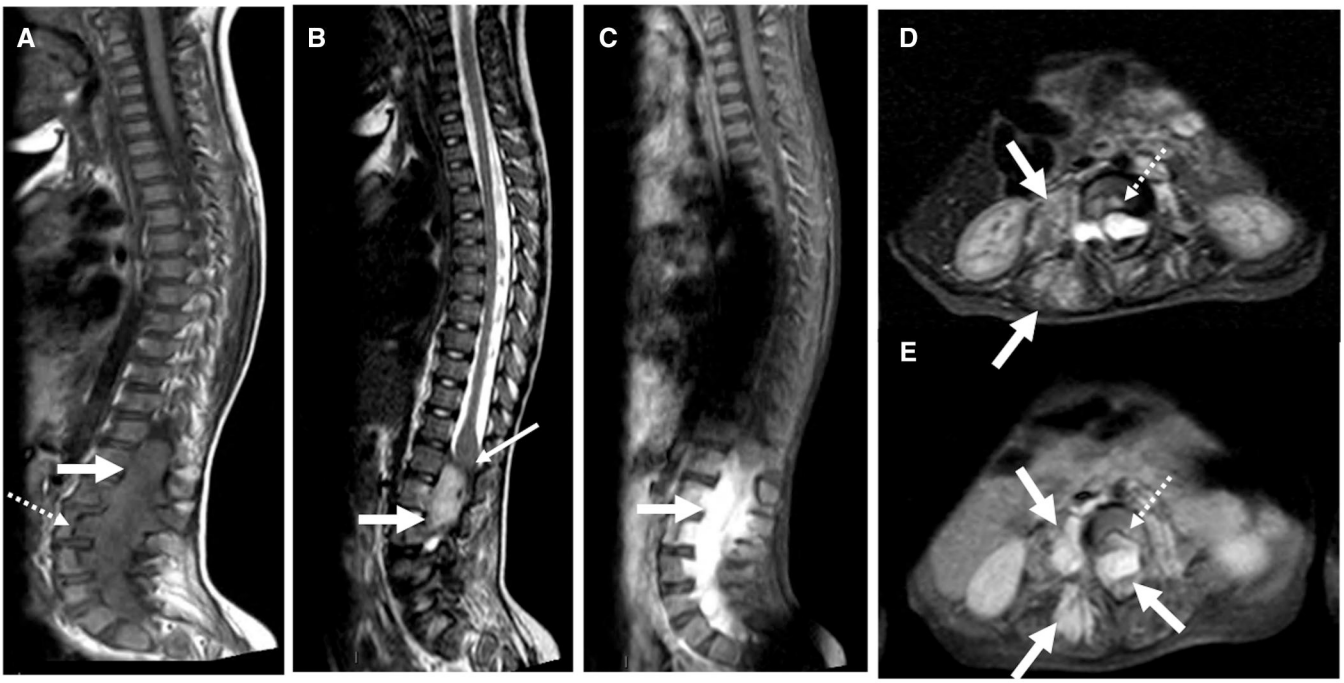

Figure 11. Para-spinal low-grade spindle cell sarcoma/lipofibromatosis-like neural tumour with the NTRK1-TPM3 fusion transcript in a 3-year-old girl. Sagittal T1 (A), T2 (B), and postcontrast T1 (C)-weighted MR images and axial T2 fat-saturated (D) and postcontrast T1 (E)-weighted MR images. They show a lumbar infiltrative mass with invasion of the paravertebral muscles and epidural tissue (thick arrow), displaying isointensity on T1-W images (A), hyperintensity on T2-W images and high homogeneous enhancement (C, E). The mass is responsible for medullar compression (arrow) and erosion of the surrounding vertebral bodies (dotted arrow).

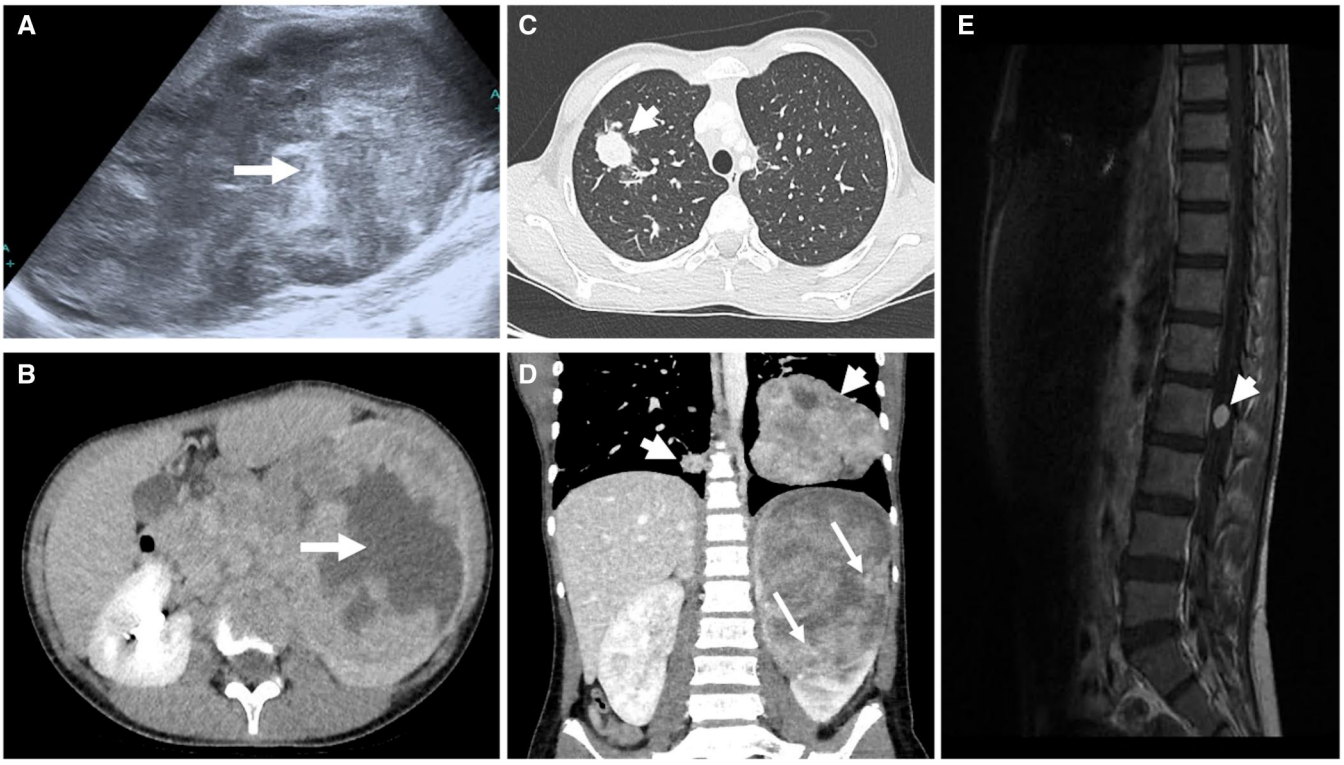

Figure 12. Undifferentiated renal sarcoma with the NTRK3-LMNA fusion transcript in a 12-year-old boy. Longitudinal greyscale US (A), axial contrast-enhanced abdominal CT in the delayed phase (B), axial thoracic CT in the pulmonary window (C), coronal contrast-enhanced abdominal CT in the portal phase (D), and sagittal postcontrast T1-weighted MR (E) images. They show a heterogeneous mass in the upper lobe of the left kidney containing a hypoechoic area and a nonenhanced hyperechoic area indicating necrotic and haemorrhagic components (thick arrow). (D) Enlarged intratumoural vessels within the lesion with irregular distribution (arrow). Note the aggressive behaviour of the tumour, with several pulmonary and intramedullary metastatic lesions (arrowhead).

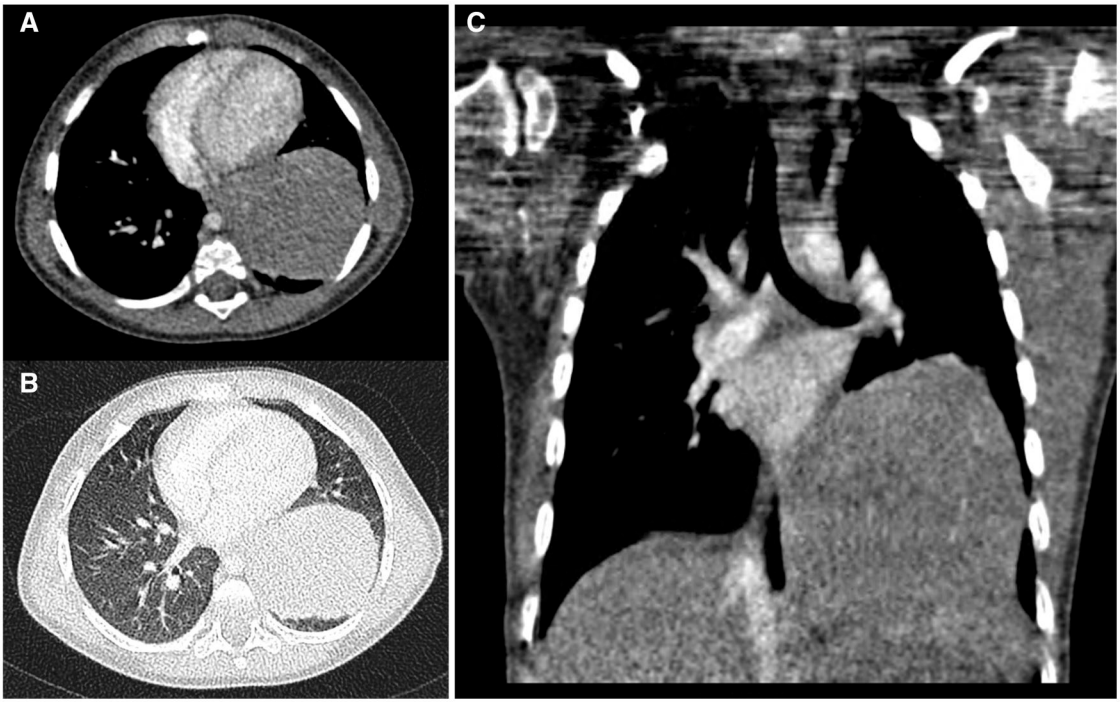

Figure 13. Inflammatory myofibroblastic tumour (ALK negative with a NTRK3-ETV6 fusion transcript) in a 15-month-old girl. Axial contrast-enhanced thoracic CT on mediastinal (A) and pulmonary (B) windows and coronal contrast-enhanced thoracic CT on the mediastinal window (C) demonstrating a homogeneous pulmonary mass with well-defined margins and low enhancement.

Figure 14. Fibular osteosarcoma with the NTRK3-CAMSAP2 fusion transcript in a 15-year-old girl. Axial CT of the leg on the bone window (A); axial T2-weighted fat-saturated MR image (B); and coronal T1 (C), T2 (D), and postcontrast T1 (E)-weighted MR images. They show an aggressive bone lesion of the fibula with a permeative periosteal reaction (thick arrow) and great extension to soft tissues (arrow), displaying high and heterogeneous signals on T2 and heterogeneous enhancement.

Interobserver agreement was not evaluated. No control cohort was used to assess distinctive radiological features between *NTRK*-FT tumours and tumours without *NTRK*-FT. Finally, the identification of imaging characteristics was not possible for exceptional cases, such as our lung and bone tumour cases.

Conclusion

NTRK-FT paediatric tumours are rare neoplasms occurring primarily in infants. IFS and cCMN have the highest prevalence, but a wide range of histotypes, such as CNS tumours and a few other benign mesenchymal tumours, is also observed. Although not constant, a high degree of

vascularization is a recurrent finding in the three most frequent anatomical locations—ie, in soft tissues, kidneys, and the brain.

Acknowledgements

We thank all the physicians at the participating centres who kindly provided clinical and radiological data

Funding

This translational research project is partially supported by Bayer (Investigation Supported research), by the French society for childhood and adolescent cancers and leukemias (SFCE) and by Imagine for Margo grant.

Conflicts of interest

None declared.

References

1. Westphalen CB, Krebs MG, Le Tourneau C, et al. Genomic context of NTRK1/2/3 fusion-positive tumours from a large real-world population. *NPJ Precis Oncol*. 2021;5(1):69. doi: 10.1038/s41698-021-00206-y
2. Knezevich SR, McFadden DE, Tao W, Lim JF, Sorensen PHB. A novel ETV6-NTRK3 gene fusion in congenital fibrosarcoma. *Nat Genet*. 1998;18(2):184-187. https://doi.org/10.1038/ng0298-184.
3. El Demellawy D, Cundiff CA, Nasr A, et al. Congenital mesoblastic nephroma: a study of 19 cases using immunohistochemistry and ETV6-NTRK3 fusion gene rearrangement. *Pathology*. 2016;48(1):47-50. https://doi.org/10.1016/j.pathol.2015.11.007.
4. Laetsch TW, DuBois SG, Mascarenhas Leo, et al. Larotrectinib for paediatric solid tumours harbouring NTRK gene fusions: phase 1 results from a multicentre, open-label, phase 1/2 study. Lancet Oncol. 2018;19(5):705-714. doi: 10.1016/S1470-2045(18)30119-0.
5. Doz F, van Tilburg CM, Geoerger B, et al. Efficacy and safety of larotrectinib in TRK fusion-positive primary central nervous system tumors. *Neuro Oncol*. 2022;24(6):997-1007. doi: 10.1093/neuonc/noab274.
6. Canale S, Vanel D, Couanet D, Patte C, Caramella C, Dromain C. Infantile fibrosarcoma: magnetic resonance imaging findings in six cases. *Eur J Radiol*. 2009;72(1):30-37. https://doi.org/10.1016/j.ejrad.2009.05.036.
7. Sargar KM, Sheybani EF, Shenoy A, Aranake-Chrisinger J, Khanna G. Pediatric fibroblastic and myofibroblastic tumors: a pictorial review. *Radiographics*. 2016;36(4):1195-1214. https://doi.org/10.1148/rg.2016150191.
8. Bayindir P, Guillerman RP, Hicks MJ, Chintagumpala MM. Cellular mesoblastic nephroma (infantile renal fibrosarcoma): institutional review of the clinical, diagnostic imaging, and pathologic features of a distinctive neoplasm of infancy. *Pediatr Radiol*. 2009;39(10):1066-1074. https://doi.org/10.1007/s00247-009-1348-9.
9. Kobayashi H, Teramura Y, Yamashita K, Makise N, Ae K, Tanaka S. Imaging findings of NTRK-rearranged spindle cell neoplasms: a case series. *Mol Clin Oncol*. 2023;18(3):14. https://doi.org/10.3892/mco.2023.2610.
10. Takamiya A, Ishibashi Y, Makise N, et al. Imaging characteristics of NTRK-rearranged spindle cell neoplasm of the soft tissue: A case report. *J Orthop Sci*. 2022;28(6):1580-1583. https://doi.org/10.1016/j.jos.2021.11.002.1
11. Dupuis M, Shen Y, Curcio C, et al. Successful treatment of lipofibromatosis-like neural tumor of the lumbar spine with an NTRK-fusion inhibitor. *Clin Sarcoma Res*. 2020;10(1):14. https://doi.org/10.1186/s13569-020-00136-6.
12. Vinnicombe SJ, Hall CM. Infantile fibrosarcoma: radiological and clinical features. *Skeletal Radiol*. 1994;23(5):337-341. https://doi.org/10.1007/BF02416988.
13. Ainsworth KE, Chavhan GB, Gupta AA, Hopyan S, Taylor G. Congenital infantile fibrosarcoma: review of imaging features. *Pediatr Radiol*. 2014;44(9):1124-1129. https://doi.org/10.1007/s00247-014-2957-5.
14. Variend S, Bax NMA, Gorp JV. Are infantile myofibromatosis, congenital fibrosarcoma and congenital haemangiopericytoma histogenetically related? *Histopathology*. 1995;26(1):57-62. https://doi.org/10.1111/j.1365-2559.1995.tb00621.x.
15. Argani P, Ladanyi M. Recent Advances in Pediatric Renal Neoplasia. *Adv Anat Pathol*. 2003;10(5):243-260. https://doi.org/10.1097/00125480-200309000-00001.
16. Gambella A, Senetta R, Collemi G, et al. NTRK fusions in central nervous system tumors: a rare, but worthy target. *IJMS*. 2020;21(3):753. https://doi.org/10.3390/ijms21030753.
17. Guerreiro Stucklin AS, Ryall S, Fukuoka K, et al. Alterations in ALK/ROS1/NTRK/MET drive a group of infantile hemispheric gliomas. *Nat Commun*. 2019;10(1):4343. https://doi.org/10.1038/s41467-019-12187-5.
18. Dangouloff-Ros V, Tauziède-Espariat A, Roux C-J, et al. CT and multimodal MR imaging features of embryonal tumors with multilayered rosettes in children. *AJNR Am J Neuroradiol*. 2019;40:732-736. https://doi.org/10.3174/ajnr.A6001.
19. Cardoen L, Tauziède-Espariat A, Dangouloff-Ros V, et al. Imaging features with histopathologic correlation of CNS high-grade neuroepithelial tumors with a *BCOR* internal tandem duplication. *AJNR Am J Neuroradiol*. 2022;43(1):151-156. https://doi.org/10.3174/ajnr.A7367.